Plasma enabled conformal and damage free encapsulation of fragile molecular matter: from surface-supported to on-device nanostructures

Maria Alcaire[1], Francisco J. Aparicio[1], José Obrero[1], Carmen López-Santos[1], Francisco J. Garcia-Garcia[1], Juan R. Sánchez-Valencia[1,2], Fabián Frutos[3], Kostya (Ken) Ostrikov[4,5], Ana Borrás[1], Angel Barranco[1*]*

Dr. Maria Alcaire, Dr. Francisco J. Aparicio, Dr. José Obrero, Dr. Carmen López-Santos, Dr. Francisco J. García, Dr. Ana Borrás, Dr. Angel Barranco
[1] Consejo Superior de Investigaciones Científicas, Instituto de Ciencia de Materiales de Sevilla (CSIC-US) c/Américo Vespucio 49, 41092, Sevilla, Spain.

Dr. Juan R. Sánchez-Valencia
[1] Consejo Superior de Investigaciones Científicas, Instituto de Ciencia de Materiales de Sevilla (CSIC-US) c/Américo Vespucio 49, 41092, Sevilla, Spain.
[2] Departamento de Física Atómica, Molecular y Nuclear, Universidad de Sevilla, Avda. Reina Mercedes, E-41012, Seville, Spain.

Dr. Fabián Frutos
[3] Dept. Física Aplicada, ETSII-Universidad de Sevilla, Avda Reina Mercedes 41012.

Prof. Kostya (Ken) Ostrikov
[4] School of Chemistry, Physics and Mechanical Engineering, Queensland University of Technology, Brisbane, QLD 4000, Australia.
[5] CSIRO-QUT Joint Sustainable Processes and Devices Laboratory, Lindfield NSW 2070, Australia.

E-mail: angel.barranco@csic.es; fjaparicio@icmse.csic.es

Keywords: Plasma nanotechnology, Nanowires, Graphene, Damage-free interfaces, Functional nanoencapsulation

Damage-free encapsulation of molecular structures with functional nano-layers is crucial to protect nanodevices from environmental exposure. With nanoscale electronic, optoelectronic, photonic, sensing and other nanodevices based on atomically thin and fragile organic matter shrinking in size, it becomes increasingly challenging to develop nano-encapsulation that is simultaneously conformal at atomic scale and does not damage fragile molecular networks, while delivering added device functionality. This work presents an effective, plasma-enabled,

potentially universal approach to produce highly-conformal multi-functional organic films to encapsulate atomically thin graphene layers and metalorganic nanowires, without affecting their molecular structure and atomic bonding. Deposition of adamantane precursor and gentle remote plasma chemical vapor deposition are synergized to assemble molecular fragments and cage-like building blocks and completely encapsulate not only the molecular structures, but also the growth substrates and device elements upon nanowire integration. The films are insulating, transparent and are conformal at sub-nanometer scale even on near-tip high-curvature areas of high-aspect-ratio nanowires. The encapsulated structures are multifunctional and provide effective electric isolation, chemical and environmental protection, and transparency in the near-UV-visible-near-infrared range. This single-step, solvent-free remote-plasma approach preserves and guides molecular building blocks thus opening new avenues for precise, atomically-conformal nanofabrication of fragile nanoscale matter with multiple functionalities.

1. Introduction

Recent advances in the synthesis of nanomaterials with outstanding properties combined with new processing technologies can lead to highly functional and highly miniaturized components and systems at increasingly lower costs.[1-10] The efficiency of nanodevices critically depends on nano-manufacturing of functional elements and their encapsulation and packaging. The role of nano-packaging is continuously increasing not only because of the need to protect the entire device from environmental factors but to also functionalize and isolate individual nanoscale device elements.

As the devices relentlessly shrink and the nanomaterials offer multiple functions, they become more fragile, and extreme care should be taken to avoid damage during encapsulation. This issue has recently become critical for multifunctional molecular matter where disruption of inter-atomic links or removal of even a small number of atoms may lead to a partial or even

full loss of functionality.[11-14] This is why damage-free encapsulation of molecular structures with protective functional nano-layers is rapidly emerging as one of the leading nanotechnologies suitable for multifunctional nanodevices, especially those operated under harsh environmental conditions.[11-18]

Widespread use of atomically thin materials such as graphene, transition metal dichalcogenides and several other classes of fragile nanoscale matter in electronic, opto- and magneto-electronic, biomedical and many other nanodevices necessitates atomically-conformal encapsulation layers.[19-22] Ideally, any sort of damage should be avoided during the fabrication. Moreover, nano-encapsulation coatings are expected to add extra functional features to the devices. As the continuously shrinking functional nanoscale elements presently exist in all dimensionalities – from zero-dimensional (0D) quantum dots to three-dimensional (3D) complex nano-architectures – the challenge to encapsulate them conformally inevitably escalates.

One particularly intriguing possibility to deliver such conformal nano-coatings is by combining damage-free deposition of customized building blocks and their guided self-assembly on the nanoscale surfaces of different dimensionalities. Indeed, manufacturing new materials through self-assembly of increasingly complex functional molecules combined with extraordinary features of nanomaterials may lead to paradigm shifts in nanodevice fabrication.[12,23-25] One such technological area is nanoelectronics where conducting and semiconducting nanostructures are coupled with state-of-the-art dielectric elements providing electrical insulation.[26-28] In organic electronics, low-κ ultrathin dielectric coatings are essential elements of advanced integrated electronic systems, and the relative permittivity κ of dielectric coatings needs to be reduced as the devices are getting smaller and smaller. Nanoporous coatings appear promising yet they often fail to protect sensitive organic nanostructures against humidity and increase their permittivity while absorbing environmental moisture.[29,30] Moreover, these and similar encapsulation coatings are commonly produced by high-

temperature deposition and/or annealing, which damage the building blocks by removing inherent polar groups or sacrificial porogens.[29,31] These factors often preclude the synthesis of such materials over temperature sensitive organic components.

Here we present a new multifunctional dielectric coating deposited by room temperature plasma-assisted vacuum deposition of adamantane. The films present remarkable properties for their applications as low-κ dielectric ultrathin films on molecular structures as protective coatings in humid and saline environments. We further demonstrate that the films can effectively encapsulate selected fragile nanomaterials of different dimensionalities, namely 1D organic conducting single-crystalline nanowires, 2D graphene monolayers, and nanoscale 3D interspaces in the supporting nanodevice platforms. The coatings are obtained by guided self-assembly of π -conjugated functional molecules, i.e., the structure is sustained by the Van der Waals forces. On the other hand, the selected molecular structures are very sensitive to damage. Indeed, the outstanding electronic photonic and magnetic properties of the organic nanowires owe to the integrity of their single-crystalline structure.[32-35] Similarly, graphene is a 2D π -conjugated system extraordinarily sensitive to defect generation. Our approach successfully addresses the key challenge to conformally encapsulate such structures while preserving their molecular arrangement and bond structure.

The key building block in our approach is a cage-like adamantane molecule - the simplest diamondoid hydrocarbon. The molecule is formed by four connected cyclohexane rings in armchair configuration with the same spatial symmetry as carbon atoms in diamond being non-polymerizable by chemical methods. Even though adamantane has been previously used for the synthesis of various diamond-like and organic films,[36-38] their use in 3D, damage-free nanoscale encapsulation has not been reported (see Supporting Information Section S1 for additional information).

Importantly, our approach is plasma-enabled and is based on basic principles of plasma nanoscience and plasma-aided nanofabrication.[39,40] We deliberately chose remote plasma assisted vacuum deposition (RPAVD) which synergizes a remote plasma discharge with low-pressure afterglow sublimation of an organic solid precursor. This approach surpasses conventional plasma polymerization by allowing the growth of a plasma polymer matrix without significant fragmentation of the precursor molecule. This is primarily due to the minimized ion bombardment and UV irradiation processes. Our results may lead to a generic approach for encapsulating molecular structures with a protective dielectric nanofilm preserving their functional properties. This approach is expected to be compatible with the wafer-scale fabrication of optoelectronic and other nanodevices.

2. Results and Discussion

2.1. Conformal thin films

Adamantane films were deposited by RPAVD according to the synthetic protocol described in the experimental section. The deposited films are insoluble in water, ethanol or acetone. The thermal stability of the films was tested up to 250 ºC in air and 350 ºC in vacuum. Thus, the films are stable at temperatures even higher than the melting point of the adamantane precursor (~210 ºC). We observed no significant variation of the films properties for a period of one year for a set of films stored in air**.**

X-ray photoemission spectroscopy and Fourier transform infrared spectroscopy (FT-IR) analysis show that the samples are almost pure hydrocarbon films formed by saturated structures with oxygen traces as low as O/C= 0.04 (see supporting information S2-S3). The films are completely transparent in the visible and ultraviolet-A (315-400 nm) regions and show an increasing absorption for wavelengths shorter than 300 nm (see Figure 1a) and the pictures in the inset). Note that, in general, plasma polymers even from unsaturated aliphatic monomers

are typically yellowish due to the presence of conjugated structures generated by the interaction of the precursor and intermediate products with the energetic plasma in the gas phase and on the surface of the growing film.[41-42] In our case, this process seems to be limited but is likely responsible for the observed UV absorption at shorter wavelengths. The pseudo band gap calculated from the Tauc relation is ~4.1 eV. The ellipsometric analysis of the films reveals a refractive index of 1.57 at 535 nm and an extinction coefficient lower than 10^{-5}.

Impedance analysis of the adamantane films is included in the supporting information S3. This analysis provides a relative permittivity value of $\varepsilon'_r \sim 2.67$ at a frequency of 10^5 Hz, which is a low value in comparison to other plasma deposited non-porous materials grown from saturated precursors.[43] From this study, it is also inferred that dipolar polarization only contributes to 10% of the sample permittivity, where the electronic polarization is the major component (S4). The low permittivity of the RPAVD Adamantane films is attributed to the apolar precursor and the soft plasma conditions which do not promote the formation of polar moieties as occurs for other plasma polymerization processes. This also justifies the low dissipation factor of the films ($\tan \delta = 0.005$).

The films are homogenous, smooth and crack free without presenting any pores, pinholes or surface aggregates observable by optical, electronic and atomic force microscopies. The atomic force microscopy (AFM) analysis reveals that the films are extremely flat with an root-mean-square (RMS) surface roughness lower than 0.3 nm. This value is independent of the film thickness in the studied range 50-750 nm (Figure S5a). These RMS values are much lower than those reported for parylene-C and polytetrafluoroethylene (PTFE) ultrathin films.[44-45] The films have a water contact angle of ~90º corresponding to a partially hydrophobic surface. This value in combination with the previously indicated low oxygen content determined for films stored in air (S2-S3) is important because low water affinity is critical for maintaining a low permittivity.[30]

The dielectric breakdown field of the adamantane films was determined using highly doped Si wafers as substrates for film deposition and evaporating an array of aluminum disk contacts onto the film surface. The films were studied as deposited after being stored in air for at least three months. Figure 1b presents the results of this characterization. The histogram accumulates the measurements of the samples with thicknesses in the range 50-110 nm precisely determined by spectroscopic ellipsometry. The dielectric breakdown strength at each point is taken as the electric field at a leakage current higher than 10^{-6} A/cm^2. The results indicate that the breakdown fields are in the range 4.5-7.3 MV/cm. These values are close to those of high-quality SiO_2, fluorinated SiO_2 and Al_2O_3 dielectric coatings, are better than other commonly used inorganic dielectrics such as Si_3N_4, and surpass dielectrics like polyethylene or PTFE (Teflon)[46-48] These values are also higher than those reported for parylene films.[48,49] The high dielectric strength values exhibited by the adamantane films are particularly interesting for nanoelectronics because of the use of these films in nanoscale encapsulation of fragile nanoscale objects as presented below.

2.2. 2D graphene layers

To demonstrate the suitability of the above layers to coat sensitive substrates and materials, adamantane films were deposited on graphene monolayers supported on SiO_2/Si(100) substrates. The AFM micrograph shows that the adamantane film coated graphene surface is homogenous and smooth without defects or voids (Figure S5) and is similar to those of films deposited on flat silicon surfaces (Figure S5). The topographic and conducting AFM images in **Figure 1**b clearly show a sharp interfacial transition from the insulating adamantane films to the conductive (Au) substrate. Notably, the figure shows that the film is homogeneous and continuous even at a thickness in the range of 10 nm.

Figure 2a shows the Raman spectra of a supported graphene monolayer after and before the adamantane film deposition. Raman spectroscopy is a reference technique for carbon-based

materials as graphene since it provides information about disorder, edge and grain boundaries, doping, thickness, etc.[50] The Raman spectra of the graphene after and before the deposition of a 100 nm adamantane film are almost identical, with only a slight change in the background at low frequencies noticeable. The intensity of the graphene D band at about 1350 nm quantifies the level of defects in graphene.[51] After background subtraction, the I_D/I_G intensity ratio is low and almost the same for the both samples. The I_D/I_G intensity ratio is a measure of the graphene crystalline quality.[52,53] Importantly, the quality of the graphene film was not affected by the adamantane coating.

Raman spectroscopy is a reference technique for carbon-based materials as graphene since it provides information about disorder, edge and grain boundaries, doping, thickness, etc.[49] The Raman spectra of the graphene after and before the deposition of a 100 nm adamantane film are almost identical, with only a slight change in the background at low frequencies noticeable. The intensity of the graphene D band at about 1350 nm quantifies the level of defects in graphene.[50] After background subtraction, the I_D/I_G intensity ratio is low and almost the same for the both samples. The I_D/I_G intensity ratio is a measure of the graphene crystalline quality.[51,52] Importantly, the quality of the graphene film was not affected by the adamantane coating.

The electrical properties at the nanoscale were studied by conductive AFM to continue exploring the possibility of using the adamantane films as conformal dielectric coatings for graphene-based devices. Figure 2b shows the local electrical characterization in the boundary region between a 90 nm thick conformal adamantane film and an uncoated region of the graphene substrate produced by using a shadow mask during the deposition. The adamantane film and graphene are in electrical contact with the evaporated Al electrode as shown in the schematics. The *I-V* curve in the (1) region (adamantane film) is characteristic of an insulating material whereas the (2) region (graphene) is characteristic of a conducting material. The *I-V* curve is very similar to those obtained before the adamantane deposition measured with the

same set-up as shown in the figure. Thus, the tested exposed graphene surface is in electrical contact with the Al electrode through the insulating organic coated region. These results are consistent with the Raman analysis indicating that the graphene monolayer structure and conductivity are not disturbed by the adamantane film deposition process. In addition, these results demonstrate that the deposition method provides a one-step, dry (solvent-free) and room temperature synthesis of conformal insulating films on conducting graphene monolayers.

The study of adamantane film growth on graphene monolayers indicates that the deposition process is conformal and soft enough for not damaging the delicate bond structure of the conducting graphene sheets. The process is thus highly-promising for applications in 2D conducting and semiconducting devices.[54]

2.3. Supported 1D organic nanowires

To extend the use of these dielectric layers within organic nanodevices, we have studied the adamantane deposition process on a 3D organic model system. This system consists of 1D small-molecule conducting organic nanowires and the 3D spaces between the nanowires and over the supporting substrates in the device platforms where the nanowires are integrated. The nanowires are obtained by molecular self-assembly.[32,55] Specifically, Cu-phthalocyanine nanowires are grown by sublimation on silver nanoparticles coated Si(100) substrates. These nanowires are single-crystalline presenting well-defined square or rectangular cross-sections. The adamantane film was deposited as a conformal shell after the nanowire synthesis in the same reactor as shown in **Figure 3**a. The planar and cross-sectional views in the figure show a dense forest of supported nano-cables formed on the substrate surface.

There are no signs of any significant nanowire damage by the adamantane deposition process. The STEM micrographs of individual nanocables in Figure 3b show regular core-shell structures with the original organic nanowires in the center. In the HRSEM image (Figure 3b right), the square-shaped core of the pristine wire can be neatly observed. The high-resolution

TEM image of a selected core-shell nanocable (Figure 3c) reveals that the adamantane films are perfectly deposited on top of the last plane of phthalocyanine molecules without producing any kind of local damage or molecular disarrangement observable even at this high magnification scale. Therefore, a sharp, well-resolved interface between the molecular planes of the crystalline nanowire and the amorphous organic films has been obtained. The Fast Fourier Transformation (FFT) analysis confirms the amorphous nature of the organic films surrounding the crystalline core. The possibility of depositing confomal films on high aspect ratio structures is one of the key properties of the RPAVD ADA deposition. In fact, conformal ADA films similar to those shown in Figure 3 have been obtained for different supported phtalocyanine nanowires in the range 1-20 micrometers long with a rectangular or square cross sections.

2.3. 3D on-device structures

The organic nanowires are conducting thus presenting ohmic behavior at small voltages.[32] **Figure 4**a) shows SEM images of a number of CuPc nanowires connecting two gold parallel planar electrodes on a glass substrate. The nanowires shown in the figure were mechanically transferred to the gold electrodes by pressing the electrodes against a supported nanowire surface. The corresponding *I-V* curve is also shown in the figure (black dots). Note that by this procedure, the nanowires are simply resting on the electrodes and thus the electrical connection is far from optimal. After this measurement, the electrodes and bridging nanowires were coated by a conformal adamantane film of about 90 nm and measured again. The resulting *I-V* curve after this treatment (blue dots) is identical to the original sample indicating that the deposition process preserves not only the nanowires integrity but also the electrical contact between the bridging wires resting on the gold electrodes.

Plasma-made adamantane nanocomposites are insoluble in water. Compared to our recent work, where the “coarse” encapsulation was demonstrated at a larger, perovskite solar cell

device scale here we increase precision and demonstrate conformal 3D encapsulation of organic nanowires with adamantane nanocoatings, which will protect them even from corrosive saline liquid environments.[56] The results corresponding to encapsulated CuPc nanowires are shown in Figure 4b). The voltammetric curves of the figure correspond to supported CuPc nanowires grown on an ITO electrode in a concentrated NaCl solution (i.e., seawater conditions ~3.5 M) after and before the deposition of an adamantane film. The bare supported nanowires working electrode show maxima and minima assigned to oxidation and reduction reactions. The anodic and cathodic peaks occurring at potentials about -0.17 V correspond to redox reaction of the Cu(II)-Pc/Cu(I)-Pc system. The lack of symmetry of these peaks and the differences between the two cycles clearly indicate the irreversibility of the process. This is rather expected considering the aggressiveness of the solution. At potentials of about 0.4 V, an additional peak appears on the curve attributed to the oxidation reaction of non-complexed copper ions. The additional peak appears only when the electrode becomes polarized with potentials over 1.1 V. At a potential of about 1.13 V, the peak of the oxidation of the complex is visible. It may indicate that this stage of oxidation still leads to the decomposition of the particles of the complex and the release of the ions of copper.

In contrast, the supported nanowire surfaces show no response at the studied voltages during the two cycles. Indeed, current density values measured on the coated sample are of about two orders of magnitude lower than the sample without adamantane. Several implications of this result are worth emphasizing. First, the coated nanowires are stable in the concentrated saline environment. Second, the adamantane film covers the nanowires fully. Thus, each nanowire is completely insulated from the tip to its foundations with a coating presenting no defects or voids. Third, the adamantane film also covers and protects (from the solution) the ITO substrate surface that supports the nanowires. In other words, the conformal deposition reaches the substrate surface below a nanowire maze similar to the cross-sectional SEM image in Figure 3a.

The facts that (i) the films conformally cover the substrates supporting the organic nanowires and (ii) the near-atomic smoothness of the coatings on flat surfaces (i.e., silicon wafers and graphene) indicate that the deposition process is determined by surface diffusion of film-forming species produced through the interaction of adamantane precursor molecules with the plasma. Note that in the absence of plasma crystallites of condensed precursor are formed in the external surface of any substrate (i.e,. at the surface of those nanowires exposed to the precursor flow). Some sections of the nanowire structure and the substrate surface are not directly exposed to the plasma and are not reachable by the molecular flow. In this unique case (cross-section in Figure 3a) the film growth cannot be attributed to common mechanisms of direct vacuum condensation of adamantane molecules or direct plasma polymerization of the precursor. We emphasize that the distance between the supported nanowires and the voids between them are much smaller than the characteristic Debye length (of the order of tens of microns range for this type of plasma discharges), which supports the plausibility of the plasma enhanced surface diffusion mechanism. [57] Thus, the role of the remote plasma is critical as it modifies the deposition process giving rise to the deposition of a conformal polymer film.

3. Conclusion

In this work, we have demonstrated an effective and potentially universal approach for highly-conformal, damage-free encapsulation of fragile nanoscale functionalities of interest to diverse applications. The approach is based on room-temperature remote plasma deposition of adamantane-derived thin transparent films. The films are ideal as versatile low-κ insulators for the nano-packaging of molecular structures and their use in electrical and optical nanodevices. The nanocomposites are chemically and thermally stable and robust in humid and saline environments. We have also shown that the dielectric films can be directly applied to graphene and conducting wires formed by the π-stacking of planar molecules. The excellent conformality of the films has been demonstrated at the nanometer scale by fully coating all the surfaces of

high-aspect-ratio supported organic nanowires, including the nanowires that connect microelectrodes on-device. Importantly, the electrical properties of the nanowires or the contacts were not affected.

The deposition process is fully compatible with the advanced shadow mask technology, plasma etching and is scalable towards multiple-wafer batch processes used in microelectronics industry. The adamantane films were deposited without any optimization cycle to further improve their dielectric or optical properties. This work thus opens multiple opportunities for further improvements of the film performance and for diversifying the range of nanoscale matter to be encapsulated, including rapidly growing areas of organic micro-and optoelectronic devices. Our results suggest significant future potential of this versatile, precise, and energy-efficient plasma-enabled platform technology in diverse fields of research and industrial applications.

Experimental Section

Adamantane is a white powder with a characteristic odor due to its relatively high vapor pressure at room temperature. High purity adamantane ($C_{10}H_{16}$) powder (>99%) were purchased from Sigma-Aldrich and used without further purification. Graphene monolayers grown by CVD and transferred to SiO_2/Si(100) substrates by wet chemistry were supplied by Graphenea.

The polymerized thin films were prepared by sublimation of the adamantane precursor in the downstream region of the Ar microwave electron cyclotron (ECR) plasma working at 150 W. The deposition Ar pressure was $1x10^{-2}$ mbar. The sample holder was placed at 12 cm from the plasma upside down with respect to the discharge to reduce the interaction with the plasma. A detailed description of the reactor geometry is included in S6 and reference [58]. Note that using this synthetic strategy it is possible to reduce very effectively the plasma interaction and fragmentation reducing effectively the fragmentation and cross-linking degree of the growing

film in comparison with conventional plasma enhanced chemical vapor deposition processes.[38, 40,58-61] Further information about the remote plasma synthesis of organic functional thin film nanocomposites can be found in previous works including a study of plasma parameters during the deposition of RPAVD films.[58,62]

Film thickness (in the range 30-300 nm) and evaporation rate were monitored by using a quartz crystal monitor placed beside the sample holder in the deposition region. Adjusting the plasma condition and geometry of the deposition process was possible to reproducibly control the thin film properties.

Planar and cross-sectional Field Emission Scanning Electron Microscopy (FESEM) images were recorded with a Hitachi S4800 microscope. The UV-Vis transmission of the films was measured with a Cary 100 spectrophotometer from Varian and the variable angle spectroscopic ellipsometric characterization with a VASE ellipsometer from J.A. Wollam Co.

Topographic atomic force microscopy images of graphene monolayers were obtained with a Cervantes AFM system from NANOTEC. Some *I-V* curves were also recorded with the same microscope by using a conductivity set-up. Note the particular shape of the *I-V* curves of the graphene monolayers determined by conductive AFM are a function of different parameters involving the nature of the tip, the different electrical interfaces in the circuit and the actual parameters used to obtain the curve. However, all these parameters were the same in all the measurements.

Scanning spreading resistance microscopy images of ADA films in gold were obtained with a Bruker-Dimension Icon AFM using Bruker DDESP-FM tips with a sample bias of -1V DC bias and an applied force of 200 nN.

The spectroscopic impedance measurements were accomplished by a custom-made two-probe setup connected to an Autolab 302N potentiostat. NOVA electrochemistry software (Metrohm Autolab) was used for data collection, equivalent-circuit design, model fitting, and data analyses.

Cyclic voltammograms were performed at room temperature in a 250 ml three-electrode cell with a computer-controlled Autolab PGSTAT302N potentiostat after stabilization of the open circuit potential was achieved (15 minutes). The CuPc fibers + Adamantane deposited on ITO substrates were used as working electrodes. All potentials were measured against and are referred to an Ag/AgCl/KCl (saturated) reference electrode, whereas a Pt foil was used as a counter electrode. Comparisons were made with CuPc fibers coated onto ITO substrates (without Adamantane). In all experiments, the electrolyte was an N_2 purged 0.6 M NaCl (Sigma-Aldrich) solution in ultrapure water (Millipore Direct-Q system, >18 MΩ cm).

Graphene monolayers supported by a SiO_2 coated Si(100) wafer form Graphenea were deposited as received without any surface cleaning procedure. The nanowires were grown on a silver-coated Si(100) wafer before the adamantane film deposition.

Raman spectra of graphene with and without adamantane coating were measured in a LabRAM Horiba Jobin Yvon HR800 confocal microscope with a He-Ne laser (532 nm) working at 10 mW as the excitation source. The spectra were recorded through a 600 grooves/mm grating by means of a 100x Objective. The Raman spectra were calibrated with respect to a reference signal collected from a Si(100) wafer.

Supporting Information

Supporting Information is available from the Wiley Online Library or from the author.

Acknowledgments

We thank MINECO-AEI and EU-FEDER for financial support (MAT2015-6903J-REDC, MAT2016-79866-R and EU-H2020-MSCA-IF-2014-661480 and Ramón y Cajal and Juan de la Cierva Programs). We also thank D. Mariolle Leti-CEA (France) for his assistance in some of the AFM characterizations (Program NFFA-Europe Translational Access). JRS-V thanks the University of Seville through the VI PPIT-US. K.O. acknowledges support from the Australian Research Council.

Conflict of Interest

The authors declare no conflict of interest.

Keywords: Plasma nanotechnology, Nanowires, Graphene, Damage-free interfaces, Functional nanoencapsulation

Received: ((will be filled in by the editorial staff))
Revised: ((will be filled in by the editorial staff))
Published online: ((will be filled in by the editorial staff))

References

[1] B. Tian, X. Zheng, T. J. Kempa, Y. Fang, N. Yu, G. Yu, J. Huang, C. M. Lieber, *Nature* **2007**, *449*, 885.
[2] J. A. Rogers, T. Someya, Y. Huang, *Science* **2010**, *327*, 1603.
[3] A. D. Franklin, *Science* **2015**, *349*, aab2750.
[4] A. G. Kelly, T. Hallam, C. Backes, A. Harvey, A. S. Esmaeily, I. Godwin, J. Coelho, V. Nicolosi, J. Lauth, A. Kulkarni, S. Kinge, L. D. A. Siebbeles, G. S. Duesberg, J. N. Coleman, *Science* **2017**, *356*, 69.
[5] Y. Wang, I. Fedin, H. Zhang, D. V. Talapin, *Science* **2017**, *357*, 385.
[6] V. Fatemi, S. Wu, Y. Cao, L. Bretheau, Q. D. Gibson, K. Watanabe, T. Taniguchi, R. J. Cava, P. Jarillo-Herrero, *Science* **2018**, *362*, 926.
[7] S. Park, S. W. Heo, W. Lee, D. Inoue, Z. Jiang, K. Yu, H. Jinno, D. Hashizume, M. Sekino, T. Yokota, K. Fukuda, K. Tajima, T. Someya, *Nature* **2018**, *561*, 516.
[8] G. Rainò, M. A. Becker, M. I. Bodnarchuk, R. F. Mahrt, M. V. Kovalenko, T. Stöferle, *Nature* **2018**, *563*, 671.
[9] M. Romera, P. Talatchian, S. Tsunegi, F. A. Araujo, V. Cros, P. Bortolotti, J. Trastoy, K. Yakushiji, A. Fukushima, H. Kubota, S. Yuasa, M. Ernoult, D. Vodenicarevic, T. Hirtzlin, N. Locatelli, D. Querlioz, J. Grollier, *Nature* **2018**, *563*, 230.
[10] Y. Liu, J. Zhang, L.-M. Peng, *Nat. Electronics* **2018**, *1*, 644.
[11] J. Rivnay, S. Inal, A. Salleo, R. M. Owens, M. Berggren, G. G. Malliaras, *Nat. Rev. Mater.* **2018**, *3*, 17086.
[12] Q. H. Wang, K. Kalantar-Zadeh, A. Kis, J. N. Coleman, M. S. Strano, *Nat. Nanotechnol.* **2012**, *7*, 699.
[13] Y. Yang, R. Huang, *Nature Electronics* **2018**, *1*, 274.
[14] G. Iannaccone, F. Bonaccorso, L. Colombo, G. Fiori, *Nat. Nanotechnol.* **2018**, *13*, 183.
[15] K. Torikai, R. F. de Oliveira, D. H. S. de Camargo, C. C. B. Bufon, *Nano Lett.* **2018**, *18*, 5552.
[16] L. Lee, K. H. Yoon, J. W. Jung, H. R. Yoon, H. Kim, S. H. Kim, S. Y. Song, K. S. Park, M. M. Sung, *Nano Lett.* **2018**, *18*, 5461.
[17] K. Chu, B. G. Song, H.-I. Yang, D.-M. Kim, C. S. Lee, M. Park, C.-M. Chung, *Adv. Funct. Mater.* **2018**, *28*, 1800110.
[18] T. Sekitani, U. Zschieschang, H. Klauk, T. Someya, *Nat. Mater.* **2010**, *9*, 1015.
[19] M. Savchak, N. Borodinov, R. Burtovyy, M. Anayee, K. Hu, R. Ma, A. Grant, H. Li, D. B. Cutshall, Y. Wen, G. Koley, W. R. Harrell, G. Chumanov, V. Tsukruk, I. Luzinov, *ACS Appl. Mater. Interfaces* **2018**, *10*, 3975.
[20] T. Takenobu, T. Takano, M. Shiraishi, Y. Murakami, M. Ata, H. Kataura, Y. Achiba, Y. Iwasa, *Nat. Mater.* **2003**, *2*, 683.

[21] T. Liu, Y. Wang, W. Zhong, B. Li, K. Mequanint, G. Luo, M. Xing, *Adv. Healthc. Mater.* **2019**, *8*, 1800939.
[22] Y. Hou, Z. Wang, C. Cai, X. Hao, D. Li, N. Zhao, Y. Zhao, L. Chen, H. Ma, J. Xu, *Adv. Mater.* **2018**, *30*, 1704131.
[23] Q. Sun, R. Zhang, J. Qiu, R. Liu, W. Xu, *Adv. Mater.* **2018**, *30*, 1705630.
[24] Z. Yuan, X. Xiao, J. Li, Z. Zhao, D. Yu, Q. Li, *Adv. Sci.* **2018**, *5*, 1700626.
[25] J. Cai, P. Ruffieux, R. Jaafar, M. Bieri, T. Braun, S. Blankenburg, M. Muoth, A. P. Seitsonen, M. Saleh, X. Feng, K. Müllen, R. Fasel, *Nature* **2010**, *466*, 470.
[26] M. Kaltenbrunner, T. Sekitani, J. Reeder, T. Yokota, K. Kuribara, T. Tokuhara, M. Drack, R. Schwödiauer, I. Graz, S. Bauer-Gogonea, S. Bauer, T. Someya, *Nature* **2013**, *499*, 458.
[27] H. Klauk, U. Zschieschang, J. Pflaum, M. Halik, *Nature* **2007**, *445*, 745.
[28] H. Moon, H. Seong, W. C. Shin, W.-T. Park, M. Kim, S. Lee, J. H. Bong, Y.-Y. Noh, B. J. Cho, S. Yoo, S. G. Im, *Nat. Mater.* **2015**, *14*, 628.
[29] W. Volksen, R. D. Miller, G. Dubois, *Chem. Rev.* **2010**, *110*, 56.
[30] C. Yuan, K. Jin, K. Li, S. Diao, J. Tong, Q. Fang, *Adv. Mater.* **2013**, *25*, 4875.
[31] C. Wu, Y. Li, M. R. Baklanov, K. Croes, *ECS J. Solid State Sci. Technol.* **2015**, *4*, N3065.
[32] A. Borras, O. Gröning, J. Köble, P. Gröning, *Adv. Mater.* **2009**, *21*, 4816.
[33] Y. Zhang, H. Dong, Q. Tang, S. Ferdous, F. Liu, S. C. B. Mannsfeld, W. Hu, A. L. Briseno, *J. Am. Chem. Soc.* **2010**, *132*, 11580.
[34] M. Macias-Montero, A. N. Filippin, Z. Saghi, F. J. Aparicio, A. Barranco, J. P. Espinos, F. Frutos, A. R. Gonzalez-Elipe, A. Borras, *Adv. Funct. Mater.* **2013**, *23*, 5981.
[35] A. N. Filippin, V. López-Flores, T. C. Rojas, Z. Saghi, V. J. Rico, J. R. Sanchez-Valencia, J. P. Espinós, A. Zitolo, M. Viret, P. A. Midgley, A. Barranco, A. Borras, *Chem. Mater.* **2018**, *30*, 879.
[36] M. Umeno, M. Noda, H. Uchida, H. Takeuchi, *Diamond Relat. Mater.* **2008**, *17*, 684.
[37] F. J. Aparicio, I. Blaszczyk-Lezak, J. R. Sánchez-Valencia, M. Alcaire, J. C. González, C. Serra, A. R. González-Elipe, A. Barranco, *J. Phys. Chem. C* **2012**, *116*, 8731.
[38] M. Alcaire, L. Cerdán, F. L. Zamarro, F. J. Aparicio, J. C. González, F. J. Ferrer, A. Borras, J. P. Espinós, A. Barranco, *ACS Appl. Mater. Interfaces* **2017**, *9*, 8948.
[39] K. Ostrikov, E. C. Neyts, M. Meyyappan, *Adv. Phys.* **2013**, *62*, 113.
[40] R. Hatakeyama, *Rev. Mod. Plasma Phys.* **2017**, 1, 7.
[41] A. Barranco, J. Cotrino, F. Yubero, T. Girardeau, S. Camelio, A. R. González-Elipe, *Surf. Coat. Technol* **2004**, *180–181*, 244.
[42] J. L. C. Fonseca, S. Tasker, D. C. Apperley, J. P. S. Badyal, *Macromolecules* **1996**, *29*, 1705.
[43] H. Jiang, L. Hong, N. Venkatasubramanian, J. T. Grant, K. Eyink, K. Wiacek, S. Fries-Carr, J. Enlow, T. J. Bunning, *Thin Solid Films* **2007**, *515*, 3513.
[44] M. Drábik, O. Polonskyi, O. Kylián, J. Čechvala, A. Artemenko, I. Gordeev, A. Choukourov, D. Slavínská, I. Matolínová, H. Biederman*, Plasma Processes Polym.* **2010**, 7, 544.
[45] J. Jakabovič, J. Kováč, M. Weis, D. Haško, R. Srnánek, P. Valent, R. Resel, *Microelectron. J.* **2009**, 40, 595.
[46] Y. Nishioka, Y. Ohji, K. Mukai, T. Sugano, Y. Wang, T. P. Ma, *Appl. Phys. Lett.* **1989**, *54*, 1127.
[47] H. Bartzsch, D. Glöß, P. Frach, M. Gittner, E. Schultheiß, W. Brode, J. Hartung, *Phys. Status Solidi (a)* **2009**, *206*, 514.
[48] A. I. Drygiannakis, A. G. Papathanasiou, A. G. Boudouvis, *Langmuir* **2009**, 25, 147.
[49] J. B. Fortin, T.-M. Lu, Thin Solid Films 2001, 397, 223.
[50] A. C. Ferrari, J. C. Meyer, V. Scardaci, C. Casiraghi, M. Lazzeri, F. Mauri, S. Piscanec, D. Jiang, K. S. Novoselov, S. Roth, A. K. Geim, *Phys. Rev. Lett.* **2006**, *97*, 187401.
[51] R. Beams, L. G. Cançado, L. Novotny, *J. Phys.: Condens. Matter* **2015**, *27*, 083002.
[52] A. C. Ferrari, D. M. Basko, *Nat. Nanotechnol.* **2013**, *8*, 235.
[53] L. M. Malard, M. A. Pimenta, G. Dresselhaus, M. S. Dresselhaus, *Phys. Rep.* **2009**, *473*, 51.

[54] A. Castellanos-Gomez, *Nature Photonics* **2016**, *10*, 202.
[55] A. Borras, O. Gröning, M. Aguirre, F. Gramm, P. Gröning, *Langmuir* **2010**, *26*, 5763.
[56] J. Idígoras, F. J. Aparicio, L. Contreras-Bernal, S. Ramos-Terrón, M. Alcaire, J. R. Sánchez-Valencia, A. Borras, Á. Barranco, J. A. Anta, *ACS Appl. Mater. Interfaces* **2018**, *10*, 11587.
[57] A. Grill, *Cold plasma in materials fabrication : from fundamentals to applications,* IEEE Press, Piscataway, NJ, USA **1994**.
[58] F. J. Aparicio, M. Alcaire, A. Borras, J. C. Gonzalez, F. López-Arbeloa, I. Blaszczyk-Lezak, A. R. González-Elipe, A. Barranco, *J. Mater. Chem. C* **2014**, *2*, 6561.
[59] A. Barranco, P. Groening, *Langmuir* **2006**, *22*, 6719.
[60] I. Blaszczyk-Lezak, F. J. Aparicio, A. Borrás, A. Barranco, A. Álvarez-Herrero, M. Fernández-Rodríguez, A. R. González-Elipe, *J. Phys. Chem. C* **2009**, *113*, 431.
[61] F. J. Aparicio, M. Holgado, A. Borras, I. Blaszczyk-Lezak, A. Griol, C. A. Barrios, R. Casquel, F. J. Sanza, H. Sohlström, M. Antelius, A. R. González-Elipe, A. Barranco, *Adv. Mater.* **2011**, *23*, 761.
[62] A. Barranco, F. Aparicio, A. Yanguas‐Gil, P. Groening, J. Cotrino, A. R. González-Elipe, *Chem. Vap. Deposition* **2007**, 13, 319.

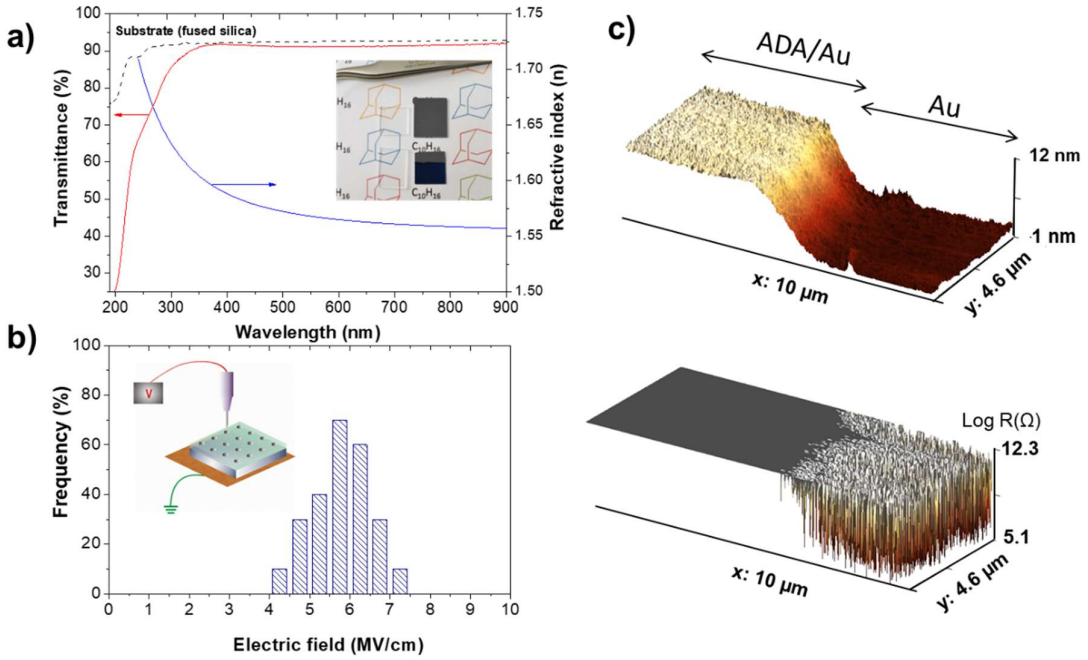

Figure 1. Electric and optical characterization of the adamantane films. a) UV-Vis transmission spectrum of a transparent adamantane film. The inset show pictures of the adamantane films on fused silica and Si(100) (bottom) and the corresponding uncoated substrates (top). Notice the uniform bluish color of the film on Si(100) due to thin film interference. b) Dielectric breakdown strength distribution of adamantane films deposited on conductive silicon wafers. c) Topographic (top) and scanning spreading resistance AFM images (bottom) corresponding to the boundaries between an ultrathin adamantane film and a gold substrate protected with a shadow mask during deposition.

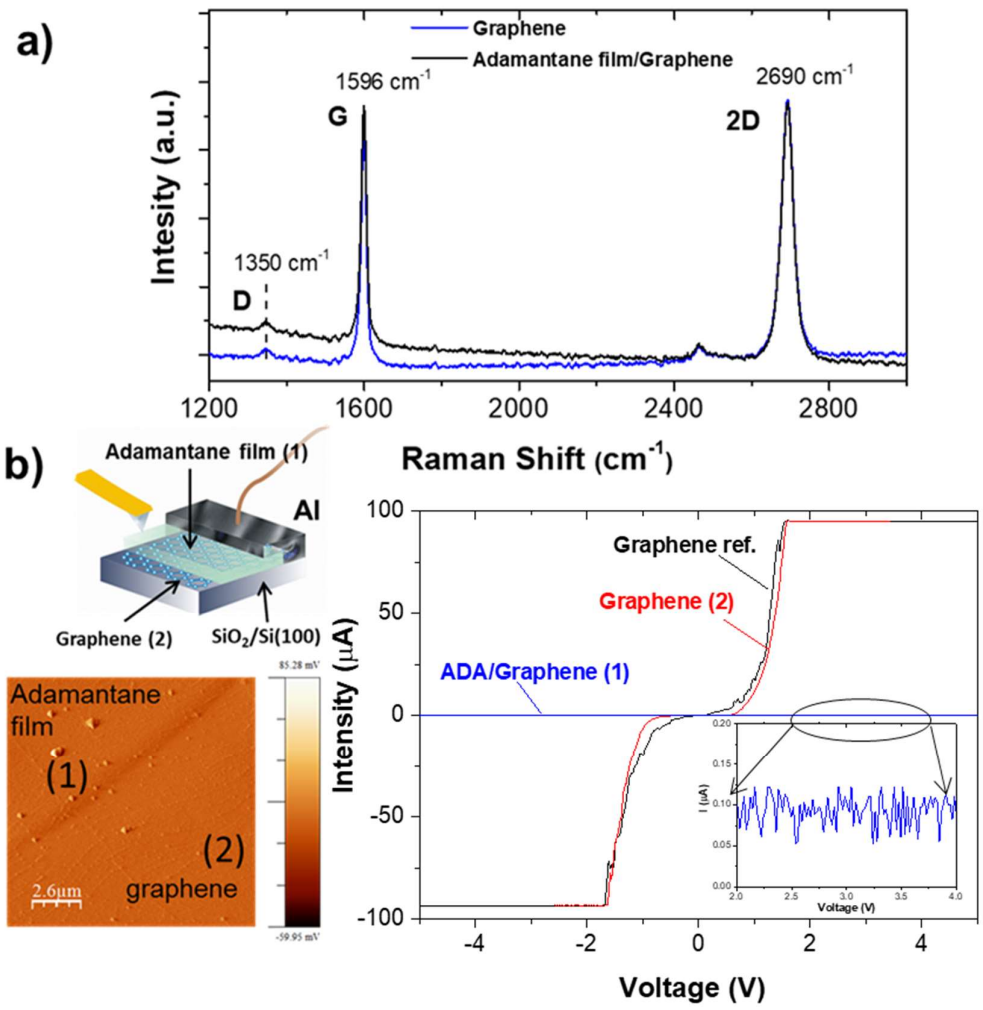

Figure 2. Adamantane films on a graphene monolayer. a) Raman spectra of a graphene monolayer after and before the deposition of *a* ~100 nm adamantane film. b) Electrical characterization curves of an adamantane film deposited on a supported graphene monolayer by using a shadow mask. The transition zone delimited by the shadow mask is shown in the AFM image. The *I-V* curves of the figure have been measured by conductive AFM according to the schematics. Region (1) corresponds to adamantane film deposited on graphene and region (2) to the uncoated graphene area as indicated.

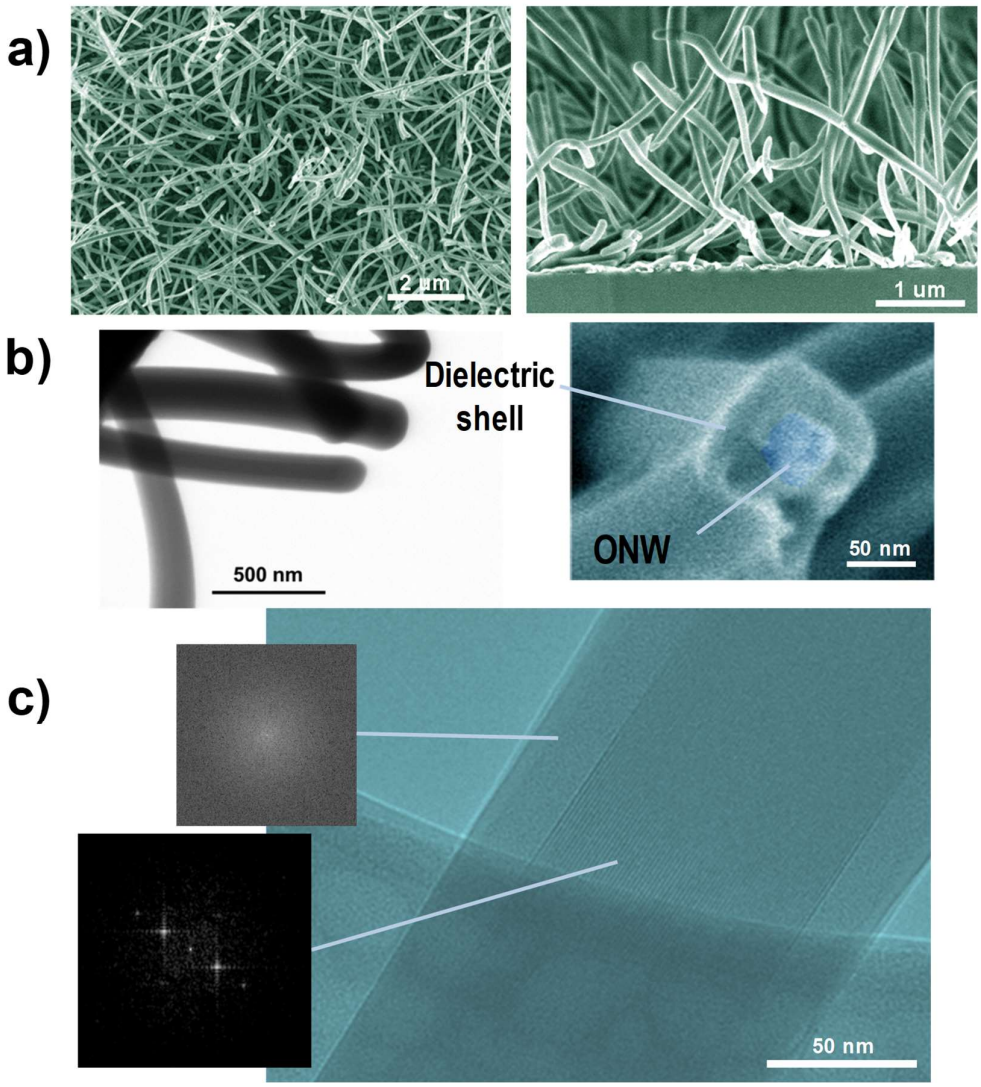

Figure 3. Conformal adamantane film deposition on organic nanowires. a) Planar and cross-sectional SEM micrographs of adamantane coated supported organic nanowire surfaces. b) STEM micrograph of adamantane coated nanowires revealing their core-shell structure. The HRSEM micrograph on the left corresponds to the section of one of these structures incidentally broken during the sample manipulation. The square-shaped core is clearly shown in false color in the center of the structure. c) HRTEM micrograph showing the section of an adamantane coated single-crystalline nanowire. A perfectly sharp interface between the molecular planes of the crystalline nanowire and the amorphous organic films can be observed. The insets correspond to the FFT patterns from the core and shell layers as indicated.

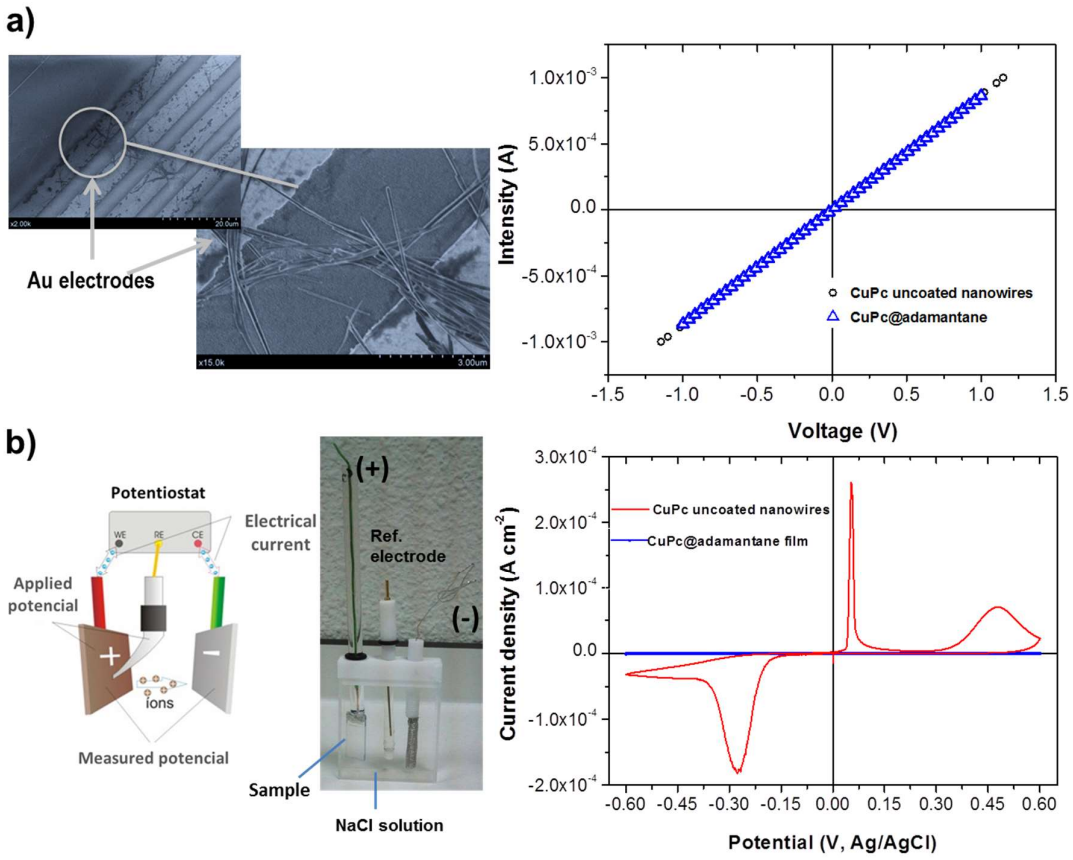

Figure 4. Electrical and electrochemical characterizations of CuPc@adamantane core-shell structures as insulated nanowires. a) The micrographs show a set of CuPc nanowires mechanically transferred to connect two parallel gold electrodes separated by 15 micrometers. The *I-V* curves correspond to this set of CuPc nanowires after and before the deposition of *a* ~100 nm thick conformal adamantane film. b) Cyclic voltammograms of a supported CuPc nanowires on ITO electrode immersed in a sodium chloride solution (3.5 M) after and before the deposition of a ~100 nm thick conformal adamantane coating. The picture and schematic show the experimental set-up for the electrochemical characterization.

Maria Alcaire[1], Francisco J. Aparicio[*], José Obrero, Carmen López-Santos, Francisco J. Garcia-Garcia, Juan R. Sánchez-Valencia, Fabián Frutos, Kostya (Ken) Ostrikov, Ana Borras, Angel Barranco[*]

Plasma enabled conformal and damage free encapsulation of fragile molecular matter: from surface-supported to on-device nanostructures

TOC figure